Removing optical artifacts in near-field scanning optical microscopy by using a three-dimensional scanning mode

Claire E. Jordan, Stephan J. Stranick, Lee J. Richter, and Richard R. Cavanagh

Citation: Journal of Applied Physics **86**, 2785 (1999); doi: 10.1063/1.371126
View online: https://doi.org/10.1063/1.371126
View Table of Contents: http://aip.scitation.org/toc/jap/86/5
Published by the American Institute of Physics

Removing optical artifacts in near-field scanning optical microscopy by using a three-dimensional scanning mode

Claire E. Jordan, Stephan J. Stranick,[a] Lee J. Richter, and Richard R. Cavanagh
Surface and Microanalysis Science Division, National Institute of Standards and Technology, Gaithersburg, Maryland 20899

(Received 28 January 1999; accepted for publication 1 June 1999)

We demonstrate a method of acquiring near-field scanning optical microscopy data that allow for the *construction* of three different types of images from one data set: topographic, constant-gap, and constant-height. This data set includes the topographic features of the surface and the optical response at various heights above the sample surface. Comparisons are made between the images recorded in this format and both conventional, constant-gap mode images, and pseudoconstant-height mode images constructed using a single retraction curve. *Z*-motion artifacts are identified by analyzing the optical intensity for a given image as a function of the sample topography. Using this procedure it is shown that significant *z*-motion artifacts exist in the constant-gap images of gold particles immobilized on a glass slide. These artifacts are avoided by constructing constant-height images. [S0021-8979(99)07517-9]

I. INTRODUCTION

Near-field scanning optical microscopy (NSOM) is a technique that can provide spatial resolution well beyond the diffraction limit of light with demonstrated resolution down to approximately $\lambda/20$.[1,2] This represents a significant improvement over the conventional optical methods. In one of the most common implementations of NSOM the high resolution is achieved by scanning a subwavelength aperture over the sample surface at a distance much less than one wavelength away from the surface. Generally the aperture is scanned while maintaining a constant gap of a few nanometers between the aperture and the sample using one of a number of types of feedback control; this is referred to as constant-gap mode (CGM) imaging. A common feedback method used in NSOM is based on shear forces between the sample and apertured probe.[3,4] A NSOM instrument based on feedback control will simultaneously provide topographic and optical information about the sample surface, making NSOM multitasked. However, operating a NSOM in this mode on rough surfaces has been shown to cause optical artifacts that often overshadow any *true* optical contrast.[5–13] These optical artifacts arise from the changing optical intensity measured as the separation between an apertured NSOM probe and the sample is varied. This results in a strong modulation of the optical signal as the probe follows a topographically rough surface. These changes in optical intensity are termed *z*-motion artifacts. A recent article by Hecht *et al.* has pointed out the prevalence of *z*-motion artifacts in the NSOM literature and suggested possible methods for their removal.[5] The methods discussed for the removal of *z*-motion artifacts are to acquire the data by scanning the NSOM probe at some set height above the average surface plane (constant-height mode, CHM) or while maintaining a constant optical intensity (constant-intensity mode, CIM), rather than using the more routinely employed CGM.

A few experiments have been reported that utilized constant-intensity or constant-height modes to collect NSOM images or to examine how the intensity changes as a function of the apertured probe-sample separation.[14–19] In one of the first applications of a three-dimensional scanning mode NSOM, Levy, Cohen, and Auschalam imaged the wavefronts that extend away from a patterned silicon surface by acquiring a series of CHM images at various heights.[17] While this approach achieved its desired goal of imaging wavefronts that extend off the surface, the scan heights used moved the surface out of the near field, degrading the achievable resolution. In another three-dimensional scanning mode NSOM application, Hatano, Inaiye, and Kauate used a scanning sequence similar to the one presented here (see experimental section) to acquire CGM line scans at various gap distances with an apertureless NSOM configuration.[16] In addition to these experiments that construct true CHM images, Weston and Buratto have described a technique that utilizes a small number of intensity scans normal to the surface, termed retraction curves, to calculate pseudo-CHM images.[11]

In this article, we report a method of collecting NSOM data that avoids *z*-motion artifacts by constructing CHM images from optical data collected in three spatial dimensions. Instead of collecting optical data with a fixed gap between the probe and the sample surface for each *XY* position, our data contains a set of optical intensities collected by controlled scans taken normal to the surface (retraction curves) at each *XY* position. Collecting data in this manner produces cubes of data such as that shown in Fig. 1(a). The three-dimensional scanning mode data contains all the information required to construct topographic, CGM, CHM, and CIM images, maintaining the multitasking capabilities of NSOM. This method of data collection also circumvents problems associated with the direct collection of CHM data: namely the uncertainties of the probe position relative to the surface that can give erroneous data and result in probe-surface con-

[a]Author to whom correspondence should be addressed; electronic mail: stephan.stranick@nist.gov

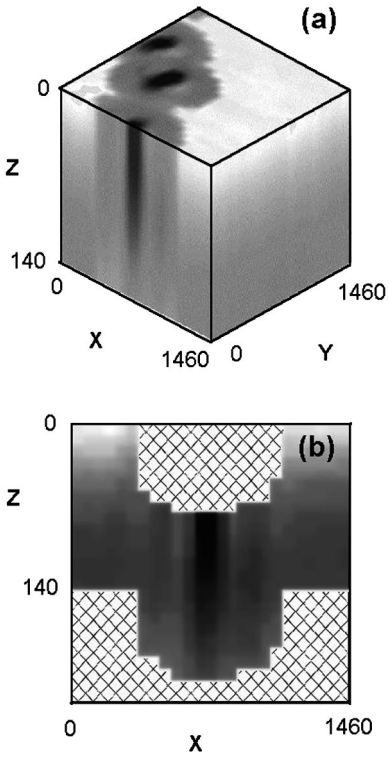

FIG. 1. NSOM data recorded in four-dimensions, three spatial dimensions (*X*,*Y*, and *Z*) and one optical dimension (transmitted optical intensity). The image cube shows the optical features of 80 nm gold particles immobilized on a silanized glass substrate. The cube covers a 1460 nm×1460 nm ×140 nm region adjacent to the sample surface with topographic changes over this area of 90 nm. In (a) the data cube is shown in acquisition coordinates and in (b) a slice at $Y=0$ is shown converted into physical coordinates by accounting for the sample topography. The hatched areas correspond to regions where no data is available either because that is where the gold particle is sitting or because the tip was retracted only 140 nm above the topography of the sample. The grayscale represents an optical intensity change from 480 to 1440 arbitrary units in (a). Note that $Z=0$ is shown at the top of the figures and corresponds to shear-force range.

tact. Also, the three-dimensional scanning mode allows one to compare all modes of operation within the same data set. This reduces the effects of systematic errors and inconsistencies that otherwise limit the comparison of different operating modes. In the sections that follow, constructed CHM images are compared with conventional CGM images and with pseudo-CHM images (generated using a single retraction curve) to understand the extent to which *z*-motion artifacts can be reduced or eliminated. In addition, a systematic method is proposed to determine if *z*-motion artifacts are present in a given image. Identifying and eliminating these artifacts should make it possible to collect meaningful NSOM images from topographically rough surfaces.

II. EXPERIMENT

In conventional scanning probe microscopes, the probe is scanned from point-to-point along a predetermined two-dimensional array of data points (nominally *XY*). During scanning, the probe measures some physical quantity, e.g., attractive or repulsive forces in atomic force microscopy, and either records this quantity or using a feedback loop responds to an error voltage that is generated based on the measured quantity. This provides topographic information about the surface. In the NSOM experiments reported here, we add controlled scans along the direction normal to the surface (*Z*) by temporarily disabling the feedback loop and applying a predetermined voltage to the *Z*-piezoelectric elements of the sample translator. These retraction curves (*Z*) are recorded at every point in the traditional *XY* scan array. By establishing shear force and recording the *Z* position of the probe between each of these retraction curves, we have the ability to construct a topographic image of the surface. This topographic image serves as the reference surface used to transform the optical data volume from acquisition coordinates [does not account for sample topography, Fig. 1(a)] into physical coordinates [sample topography is accounted for, Fig. 1(b)], which is required to construct the CHM images.

The following algorithm was used to transform the data from the acquisition coordinates into physical coordinates and then construct CHM images. First, any sample tilt was corrected for by subtracting a plane from the topographic image of the surface. Next, topographic *XYZ* coordinates are used to place the optical intensities in their appropriate position in physical space. Once the data is transformed to physical coordinates and a linear interpolation of the optical intensities measured in the *Z* direction has been performed, a slice through the optical data volume parallel to the average surface plane produces a CHM image. The only other image correction performed during data acquisition or analysis is interpolation between *XY* points to make the images appear less pixelated.

As in all scanned probe measurements, the accuracy of the data is limited by the uncertainty in the scanner position and stability. Both the *XY* positioning and the probe-sample separation must remain stable over long periods in order for these measurements to be made (at present a 25×25×25 cube takes ~2.5 h to acquire). The microscope is designed to be thermally stable, and the control electronics, namely the feedback system, are stabilized for low set point and sample-and-hold drifts (*XY* drift <0.17 nm per min and the *Z* drift during sample-and-hold mode is 0.2 nm during a 15 s retraction curve before shear force is reestablished).

The microscope design has been described in detail elsewhere.[20] In brief, the 488 nm light from an Ar^+ ion laser is coupled into an aluminum-coated, tapered optical fiber which serves as the illumination mode apertured probe. The aperture diameter for the probe used in these particular experiments is estimated to be 150 nm.[21] Distance control between the sample and the probe is achieved via electronic detection of shear-force damping of the probe and a beetle-style scanner assembly is used to control the sample position. The transmitted light is collected by a 0.55 numerical aperature optic and detected using an amplified Si PIN diode. The samples consist of Au nanoparticles, immobilized on glass coverslips silanized with 3-aminopropyl-trimethoxysilane.[22,23] The Au particles used were nominally 80 nm particles from Goldmark Biologicals.[24]

III. RESULTS AND DISCUSSION

Figure 1 shows a set of NSOM data collected in four dimensions, three spatial (*X*, *Y*, and *Z*) and one optical (trans-

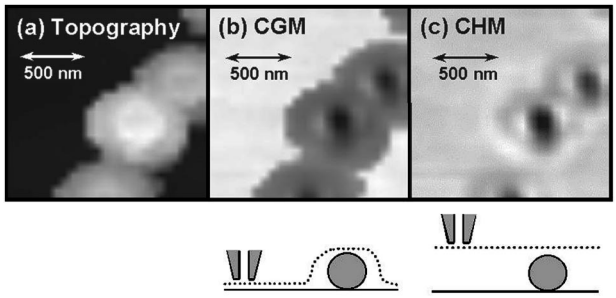

FIG. 2. Images constructed from the data shown in Fig. 1: (a) topographic, (b) CGM, and (c) CHM. The cartoons underneath (b) and (c) show a particle sitting on a glass substrate. The dotted lines indicate the approximate path that a probe would follow in CGM or CHM scanning and identify the positions from which the intensity values are taken to construct CGM and CHM images. The scan area for all three images is 1460 nm×1460 nm. The gray scale represents a topography change of 90 nm in (a) a change in transmitted intensity from 480 to 1440 a.u. in (b), and a change in transmitted intensity from 510 to 1080 a.u. in (c). The fly height for the constructed CHM image in (c) is 102 nm.

mission) as described in Sec. II. In these images the optical intensity is represented by the gray scale. Figure 2 shows three images constructed from the NSOM data shown in Fig. 1: topography, CGM, and CHM. By definition, in CGM a fixed separation between the probe and sample is maintained and the optical intensity is measured at each point on the sample surface. For CHM the optical intensity is measured at a set distance (or fly height) above the average surface. Beneath Figs. 2(b) and 2(c) are cartoons showing a gold particle on a glass surface. The dotted lines indicate the path that a probe would follow in CGM or CHM scanning and identify the relative points from which optical intensities are taken for the construction of CGM and CHM images. It has been pointed out previously that the *z*-motion artifacts, which are prevalent in CGM imaging, can be avoided by using CHM imaging.[5,13] The presence of *z*-motion artifacts in CGM and not in CHM images can be understood by considering the formalism presented by Greffet and Carminati.[13] They separate the signal (S) measured in a NSOM experiment into two contributions

$$S(x,y,z)=S^0(z)+S^1(x,y,z). \tag{1}$$

S^0 is the signal detected when scanning a flat background or substrate and it is a function only of the probe-sample separation (z). S^1 is the differential signal resulting from a sample that adds lateral structure to the substrate, i.e., from scattering processes. For a CHM image where the optical intensity is measured at a set fly height (z_0) above the average surface Eq. (1) becomes

$$S(x,y,z_0)=S^0(z_0)+S^1(x,y,z_0). \tag{2}$$

However in a CGM image Eq. (1) becomes

$$S[x,y,F(x,y)]=S^0[F(x,y)]+S^1[x,y,F(x,y)], \tag{3}$$

where $F(x,y)$ describes the z position of the probe as determined by the topography of the surface. The *z*-motion artifact in the CGM images appears as $F(x,y)$ in Eq. (3). Since the CHM signal described in Eq. (2) depends on z_0 and not on $F(x,y)$ CHM images are not subject to *z*-motion artifacts.

The effect of imaging the immobilized 80 nm gold particles with the blunt structure of an apertured NSOM probe can be seen in the topographic image, Fig. 2(a). The ~750-nm-wide features found in this image are representative of the structure of the probe and not of the true surface structure, as is expected when a probe which is larger than the particles is used for imaging.[25] The constructed CGM image is shown in Fig. 2(b) and a CHM image constructed at a fly height of 102 nm is shown in Fig. 2(c). The CHM image is constructed just above the highest topographic feature in order to produce the best resolution. For this data it is observed that the size of the optical features in a CHM image increase by about a third when the fly height is increased by 40 nm.

Many of the features present in the topographic image, Fig. 2(a), map directly into features in the CGM image, Fig. 2(b). Since *z*-motion artifacts often cause a direct correlation between optical and topographic features it is expected that many of these features are artifacts. In the constructed CHM image shown in Fig. 2(c) it is seen that the majority of the probe-size features observed in Fig. 2(b) are no longer present, indicating that these features in Fig. 2(b) result from *z*-motion artifacts. The prominent features observed for each particle in Fig. 2(c) consist of a dark center spot surrounded by two lighter lobes. In a previous article these features were compared with theoretical findings and were shown to represent true optical contrast.[21]

Some low contrast residual probe-sized features still remain in Fig. 2(c), it is not clear from this image whether these features are due to inaccuracies in the construction of the CHM image, or if they result from interference or other mesoscale optical effects.[12] Possible reasons for inaccuracies in the construction include the necessity to interpolate optical intensities in the Z direction because of the finite number of points sampled and possible material dependent variations in the probe-sample separation when the tip is in shear-force feedback. While shear-force changes due to material contrast are believed to be small,[14] typically resulting in $\ll 1$ nm change in the Z direction, and interpolation errors can be avoided with sufficient sampling, identifying possible errors in the construction is important. This makes it particularly desirable to have a systematic method, besides comparing the visual appearance of two images, to determine the degree to which *z*-motion artifacts exist in an image.

One such method of testing for *z*-motion artifacts is to plot the optical intensity (recorded in CGM or CHM) as a function of the topography at each *XY* point. This has been done in Fig. 3 for the optical intensity from the CGM and the CHM images in Fig. 2. Note that topography refers to the actual height of the surface features and that we have this information for our CHM image because it was collected using a three-dimensional scanning mode. For CGM images a plot of the optical intensity versus topography will show *z*-motion artifacts in the background signal $\{S^0[F(x,y)]\}$ plus *z*-motion artifacts and true optical contrast in the sample signal $\{S^1[x,y,F(x,y)]\}$. To understand the functional form of artifacts in such plots it is useful to remember that *z*-motion artifacts result from a combination of the functional form of the retraction curves[26] and any spatial offset between the optical aperture and the shear-force asperity.[5] Since there

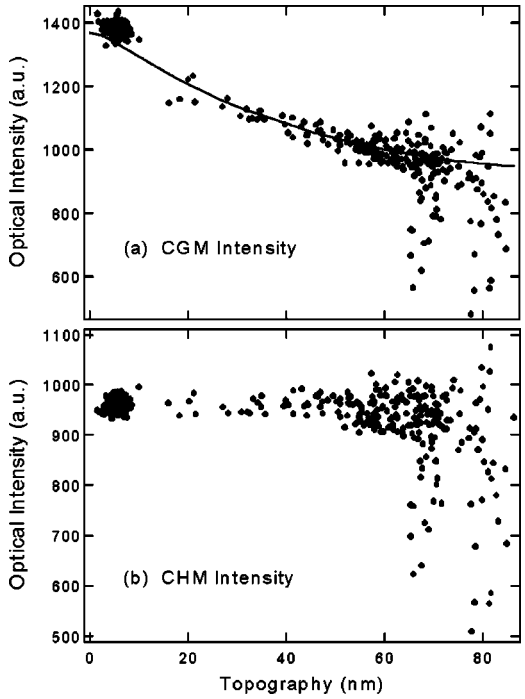

FIG. 3. Scatter plots of the detected optical intensity as a function of topography for the constructed CGM (a) and CHM (b) images in Fig. 2. The solid line in (a) is a retraction curve measured over a bare glass portion of the sample surface. The shape of the scatter plots can be used to identify the presence of *z*-motion artifacts in an image.

is typically an offset between the shear-force asperity and optical aperture, as the probe moves over a topographic feature in CGM the probe will retract away from the surface before the optical aperture is above that feature. This causes an increase in the distance between the aperture and sample and a modulation of the detected optical signal. As a result of this modulation, if *z*-motion artifacts are present in an image, a plot of optical intensity versus topography will mimic the shape of a retraction curve, or multiple retraction curves if the surface consists of different materials. For most NSOM configurations the shape of retraction curves is a combination of near-field contributions and cavity modes.[10,26–28] A plot of the optical intensity versus topography may appear to have a positive slope, a negative slope, or even sinusoidal contributions when *z*-motion artifacts are present. In general, true optical contrast will appear as points scattered away from this smooth curve.

CHM images are not subject to *z*-motion artifacts and a plot of the optical intensity versus topography is expected to show a line with a slope of zero at the optical intensity of the background signal $[S^0(z_0)]$, where deviations away from this flat line result from true optical contrast $[S^1(x,y,z_0)]$. Looking at Fig. 3(a) the slope of the optical intensity versus topography points suggests that there are significant *z*-motion artifacts in the CGM image shown in Fig. 2(b). This is confirmed by the overlap of the data points and the solid line, which is a retraction curve measured over a flat glass portion of the sample. However, Fig. 3(b) which is a plot of the optical intensity from the constructed CHM image versus topography, shows a line with a slope of zero indicating that within the signal-to-noise of our experiment *z*-motion artifacts are not present in this constructed CHM image.

Although collecting four-dimensional data and constructing CHM images is an effective method of avoiding *z*-motion artifacts, the data collection is time consuming. The data from which the images in Fig. 2 were constructed took approximately 2.5 h to collect. A faster method is to collect a retraction curve for only one *XY* point and calculate pseudo-CHM images from a CGM image and the single retraction curve, as has been done previously by Weston and Buratto for a combined illumination and collection mode apertured probe[11] and others for apertureless probes.[29,30] However, this method will result in errors with a magnitude that depends on the particular sample being studied. The origin of these errors can be understood by examining Eq. (3) where the term related to *z*-motion artifacts, $F(x,y)$, appears in *both* the S^0 and S^1 terms. While a retraction curve taken over the background substrate, $S^0(z)$, can be used to eliminate *z*-motion artifacts as described by $F(x,y)$ by removing the $F(x,y)$ dependence from the S^0 term, this retraction curve cannot be used to remove the $F(x,y)$ dependence from the S^1 term, so a single retraction curve will not remove *z*-motion artifacts over the entire sample surface.

To demonstrate this point a constructed CHM image and a calculated pseudo-CHM image of the 80 nm gold particles on glass are compared. The CHM image shown in Fig. 2(c), which was constructed using all the retraction curves measured at each *XY* point, is compared to a pseudo-CHM image calculated from the same data set but using only a single retraction curve measured above the bare glass substrate. The image in Fig. 4(a) shows the difference in optical intensity between the CHM images obtained using these two methods normalized to the optical intensity measured in Fig. 2(c). Figure 4(b) displays the optical intensity along the line indicated in Fig. 4(a). From Fig. 4(b) it can be seen that at some points there is as much as a 20% difference in the optical intensity obtained by constructing the CHM image with multiple retraction curves compared to correcting a CGM image using a single retraction curve.

The origin of this error can be better understood by examining Fig. 4(c) which plots the retraction curves collected for every second *XY* point for this data set. It can be seen from the plot that while most of the retraction curves are similar and can be represented by $S^0(z)$, a few deviate significantly from the main cluster. These are the retraction curves measured above the gold particles and include contributions from $S^1(x,y,z)$. Since a retraction curve above a gold particle differs significantly from a retraction curve collected above glass, trying to remove *z*-motion artifacts by a single retraction curve correction will introduce significant errors in areas containing gold particles. As seen in Fig. 4(a) the largest differences between the constructed CHM image and the pseudo-CHM image are in the area above the two adjacent gold particles that have a 15 nm height difference. In addition to problems with pseudo-CHM images still having some *z*-motion artifacts, the single retraction curve method also produces artificially high resolution in the resulting image. That is, the resolution in a pseudo-CHM image will be higher then the resolution in a true CHM image. This anomalously high resolution results because the single

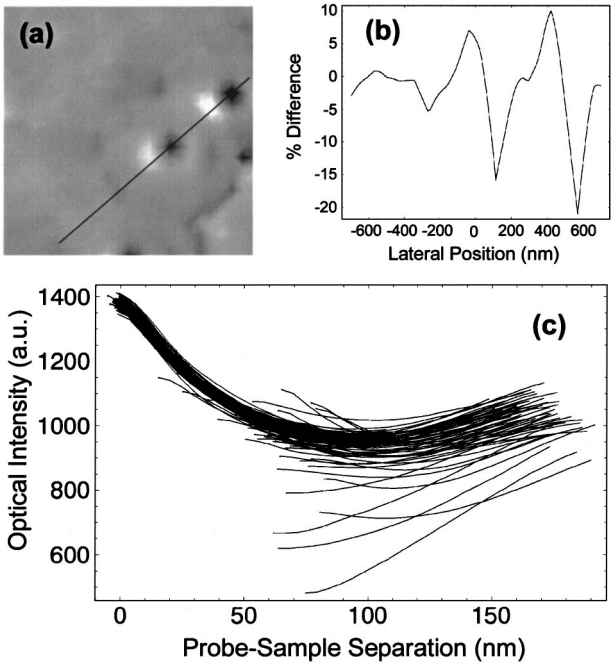

FIG. 4. Comparison of the CHM image shown in Fig. 2(c), which was constructed using the retraction curves measured at every *XY* point and a pseudo-CHM image calculated from the same data set but using only a single retraction curve measured above the glass substrate. Image (a) shows the difference in the optical intensity of the CHM image and the pseudo-CHM image, normalized to Fig. 2(c). A plot of the optical intensities measured along the solid line drawn in (a) is shown in (b). Shown in (c) is a plot of representative retraction curves measured at every fourth point on the sample surface.

retraction curve method cannot account for the fact that in a true CHM image the resolution will depend on how far the fly height for the CHM image is above a given feature. Since the pseudo-CHM image is derived from a CGM image, where the probe is always in the near field of the surface, it will have artificially higher spatial resolution than a true CHM image.

For this particular sample the errors introduced by calculating pseudo-CHM images from a single retraction curve approach 20%. For some samples and applications the errors introduced by calculating pseudo-CHM images may be small enough that they do not present difficulties and in these instances calculating pseudo-CHM images is an attractive alternative for more rapid data collection. However, the collection of three-dimensional scanning mode data and use of multiple retraction curves is a robust method of constructing CHM images, and improvements in the acquisition algorithm should significantly shorten data acquisition times. The ability to reliably identify and eliminate *z*-motion artifacts in NSOM images by constructing CHM images holds promise for the successful interpretation of NSOM data from rough surfaces.

IV. CONCLUSIONS

In this article, we have implemented a scanning mode in which optical retraction curves are recorded for each point in a two-dimensional (*XY*) scan array above the sample. This three-dimensional scanning mode of data collection allows for the construction of a topographic image of the surface as well as both CGM and CHM optical images. The utility of this method of data collection is demonstrated through the elimination of *z*-motion artifacts by constructing a CHM image of a structured sample surface. It is also shown that by plotting the optical intensity as a function of topography it is possible to qualitatively determine if *z*-motion artifacts are present in an image. Finally, comparisons are made between CHM images and pseudo-CHM images highlighting the intrinsic nature of *z*-motion artifacts in CGM images.

ACKNOWLEDGMENTS

The authors would like to thank Prof. Michael J. Natan and Dr. Chris Keating of the Pennsylvania State University, Department of Chemistry for providing the Au particle samples used in this study.

[1] U. Durig, D. W. Pohl, and F. Rohner, J. Appl. Phys. **59**, 3318 (1986).
[2] E. Betzig and J. K. Trautman, Science **257**, 189 (1992).
[3] E. Betzig, P. L. Finn, and J. S. Weiner, Appl. Phys. Lett. **60**, 2484 (1992).
[4] R. Toledo-Crow, P. C. Yang, Y. Chen, and M. Vaez-Iravani, Appl. Phys. Lett. **60**, 2957 (1992).
[5] B. Hecht, H. Bielefeldt, Y. Inouye, D. W. Pohl, and L. Novotny, J. Appl. Phys. **81**, 2492 (1997).
[6] V. Deckert, D. Zeisel, R. Zenobi, and T. Vo-Dinh, Anal. Chem. **70**, 2646 (1998).
[7] S. I. Bozhevolnyi, J. Opt. Soc. Am. B **14**, 2254 (1997).
[8] C. Durkan and I. V. Shvets, J. Appl. Phys. **83**, 1171 (1998).
[9] H. Bielefeldt, I. Horsch, G. Krausch, M. Luxsteiner, J. Mlynek, and O. Marti, Appl. Phys. A: Solids Surf. **59**, 103 (1994).
[10] G. A. Valaskovic, M. Holton, and G. H. Morrison, J. Microsc. **179**, 29 (1995).
[11] K. D. Weston and S. K. Buratto, J. Phys. Chem. B **101**, 5684 (1997).
[12] O. J. F. Martin, C. Girard, and A. Dereux, J. Opt. Soc. Am. A **13**, 1801 (1996).
[13] J. J. Greffet and R. Carminati, Prog. Surf. Sci. **56**, 133 (1997).
[14] R. L. Williamson, L. J. Brereton, M. Antognozzi, and M. J. Miles, Ultramicroscopy **71**, 165 (1998).
[15] J. P. Goudonnet, E. Bourillot, P. M. Adam, F. Defornel, L. Salomon, P. Vincent, M. Neviere, and T. L. Ferrell, J. Opt. Soc. Am. A **12**, 1749 (1995).
[16] H. Hatano, Y. Inouye, and S. Kawata, Opt. Lett. **22**, 1532 (1997).
[17] J. Levy, A. Cohen, and D. D. Awschalom, Rev. Sci. Instrum. **66**, 3385 (1995).
[18] B. Hecht, H. Bielefeldt, D. W. Pohl, L. Novotny, and H. Heinzelmann, J. Appl. Phys. **84**, 5873 (1998).
[19] D. Barchiesi, O. Bergossi, C. Pieralli, and M. Spajer, Ultramicroscopy **71**, 361 (1998).
[20] S. J. Stranick, L. J. Ritcher, and R. R. Cavanagh, J. Vac. Sci. Technol. B **16**, 1948 (1998).
[21] L. J. Richter, C. E. Jordan, R. R. Cavanagh, G. W. Bryant, A. Liu, S. J. Stranick, C. D. Keating, and M. J. Natan, J. Opt. Soc. Am. A (in press).
[22] K. C. Grabar, K. R. Brown, C. D. Keating, S. J. Stranick, S. L. Tang, and M. J. Natan, Anal. Chem. **69**, 471 (1997).
[23] K. R. Brown and M. J. Natan, Langmuir **14**, 726 (1998).
[24] Certain commercial equipment or materials are identified to adequately specify the experimental procedure. This does not imply endorsement by the National Institute of Standards and Technology or that these are the best materials or equipment for the purpose.
[25] U. D. Schwarz, H. Haefke, P. Reimann, and H. J. Guntherodt, J. Microsc. **173**, 183 (1994).
[26] C. Obermuller, K. Karrai, G. Kolb, and G. Abstreiter, Ultramicroscopy **61**, 171 (1995).
[27] C. E. Jordan, S. J. Stranick, and R. R. Cavanagh, Surf. Sci. (in press).
[28] T. Huser, L. Novotny, T. Lacoste, R. Eckert, and H. Heinzelmann, J. Opt. Soc. Am. **16**, 141 (1999).
[29] H. F. Hamann, A. Gallagher, and D. J. Nesbitt, Appl. Phys. Lett. **73**, 1469 (1998).
[30] Y. Martin, F. Zenhausern, and H. K. Wickramasinghe, Appl. Phys. Lett. **68**, 2475 (1996).